iScience

CellPress
OPEN ACCESS

Article

A facile method for separating fine water droplets dispersed in oil through a pre-wetted mesh membrane

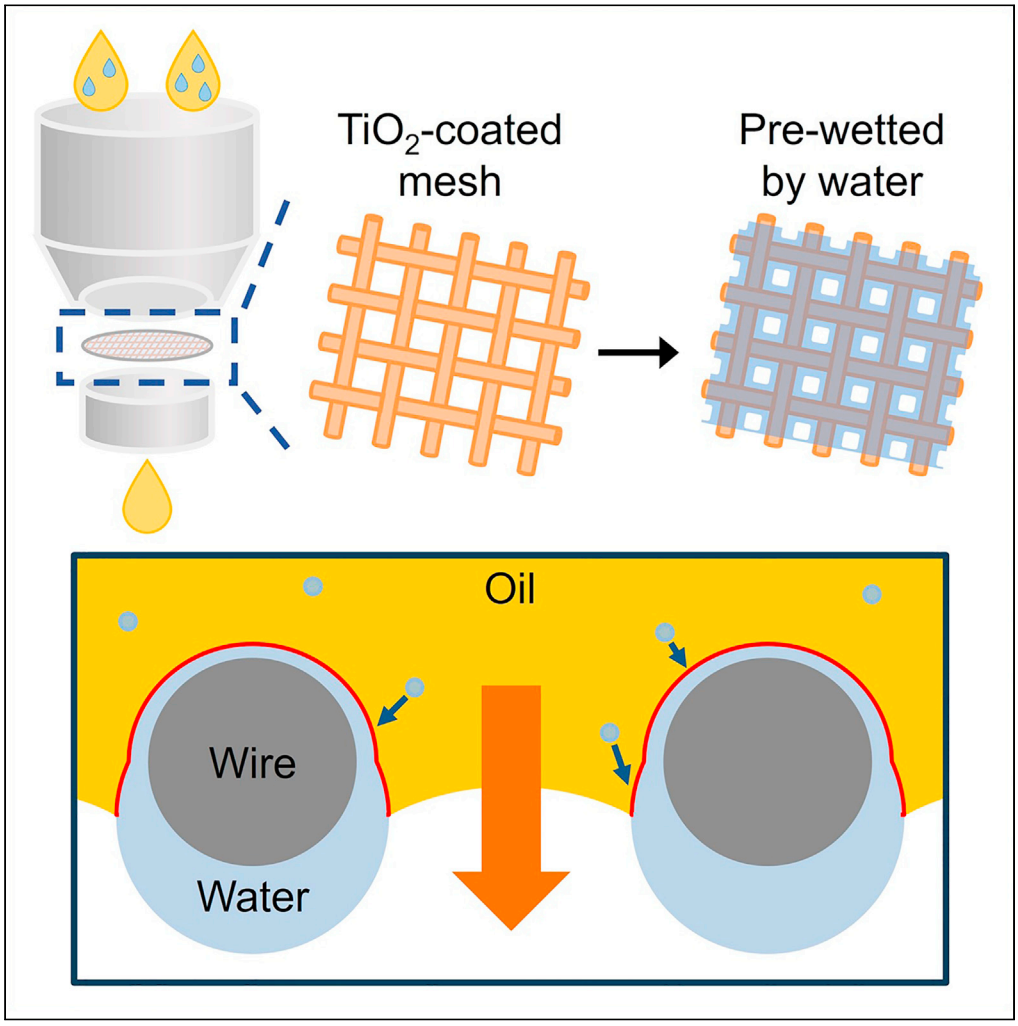

JiEun Park, Seunghan Kang, EunSol Park, ..., Donghun Kim, Siyoung Q. Choi, KyuHan Kim

donghun99@chonnam.ac.kr (D.K.)
sqchoi@kaist.ac.kr (S.Q.C.)
kyuhankim@seoultech.ac.kr (K.K.)

Highlights

A stainless-steel mesh pre-wetted by water is successfully prepared

The pre-wetted membrane retains empty pores

The membrane efficiently separates water droplets in oil with over 98% efficiency

The strategy is applicable for water volume fractions below 0.125 vol %

Park et al., iScience 27, 109556
April 19, 2024
https://doi.org/10.1016/j.isci.2024.109556

iScience

CellPress
OPEN ACCESS

Article

A facile method for separating fine water droplets dispersed in oil through a pre-wetted mesh membrane

JiEun Park,[1] Seunghan Kang,[2] EunSol Park,[1] Dongho Lee,[3] Jeasung Park,[4] Donghun Kim,[5,*] Siyoung Q. Choi,[2,*] and KyuHan Kim[1,6,*]

SUMMARY

To achieve the successful separation of emulsions containing fine dispersed droplets and low volume fractions, a membrane with pore sizes comparable to or smaller than the droplet size is typically required. Although this approach is effective, its utilization is limited to the separation of emulsions with relatively large droplets. To overcome this limitation, a secondary membrane can be formed on the primary membrane to reduce pore size, but this can also be time-consuming and costly. Therefore, a facile and effective method is still required to be developed for separating emulsions with fine droplets. We introduce a pre-wetted mesh membrane with a pore size significantly larger than droplets, easily fabricated by wetting a hydrophilic stainless-steel mesh with water. Applying this membrane to emulsion separation via gravity-driven flow confirms a high efficiency greater than 98%, even with droplets approximately 10 times smaller than the pore size.

INTRODUCTION

The presence of water droplets in oil or oil droplets in water can adversely affect various industries and environments.[1–4] For example, the emission of oily wastewater, which has substantially increased due to industrial growth, can serve as a representative example, leading to environmental pollution and interfering with the normal operation of ecosystem.[1] Oil leaks into the sea from oil spills have also frequently occurred,[2] and, as a result, crude oil droplets can accumulate in the embryos of marine fish species, thereby resulting in abnormal development.[3] In addition, water droplets formed in deep-sea pipelines create an oil-water interface conducive to the growth and aggregation of gas hydrates, eventually leading to pipeline flow blockages.[4]

Among these, the system that contains micro-sized fine water droplets in oil has considerably attracted attention in recent days.[5–8] In particular, in the petroleum industry, micro-sized fine water droplets are formed during the oil drilling process, and these droplets can be easily stabilized by natural emulsifiers in crude oil.[5] This reduces the quality of crude oil itself and further causes operating problems such as tripping of separation equipment in gas/oil separating plants, creating high pressure drops in flow lines, corrosion, and microorganism growth in the wetted part of the equipment.[5–7] Additionally, as a representative plastic recycling process, plastic pyrolysis oil has recently gained popularity. However, a small amount of water typically remains in the pyrolysis oil during the process, potentially reducing ignition performance and causing engine rust.[8]

Accordingly, to achieve effective separation of oil and water, numerous separation techniques have been developed so far. Conventional methods such as gravity separation and centrifugation can be considered the most representative ones. Here, gravity separation is driven by the difference in density between water and oil. This method has a low operating cost, but the separation time can be lengthy.[9,10] In contrast, centrifugation uses centrifugal force to separate oil and water phases by moving low-density liquids toward the centrifugal axis and high-density liquids in the opposite direction. This process is simple but requires a lot of energy when the difference in density is small.[11,12] Furthermore, their usage can be limited for separating relatively large droplets. Other methods, such as chemical demulsification and electro-coalescence, have also been applied to induce the coalescence of emulsion droplets by adding demulsifiers and applying an electric field, respectively. However, they still have respective disadvantages, such as the high cost of chemicals and the possibility of secondary fine droplet formation.[13,14] Therefore, in recent decades, membrane filtering processes have emerged due to relatively low cost and high energy efficiency.[15,16]

[1]Department of Chemical and Biomolecular Engineering, Seoul National University of Science and Technology (SeoulTech), Seoul 01811, Republic of Korea
[2]Department of Chemical and Biomolecular Engineering, KAIST, Daejeon 34141, Republic of Korea
[3]Process R&D center, Hanwha solutions R&D institute, Daejeon 34128, Republic of Korea
[4]Green and sustainable materials R&D department, Korea institute of industrial technology (KITECH), Cheonan 31056, Republic of Korea
[5]School of Chemical Engineering, Chonnam National University, Gwangju 61186, Republic of Korea
[6]Lead contact
*Correspondence: donghun99@chonnam.ac.kr (D.K.), sqchoi@kaist.ac.kr (S.Q.C.), kyuhankim@seoultech.ac.kr (K.K.)
https://doi.org/10.1016/j.isci.2024.109556

According to the separation mechanism, the membrane filtration process can be divided into size sieving and coalescing separation.[17] Size sieving primarily works based on the size difference between membrane pores and emulsions droplets. If the pore size is larger than the droplet diameter, high flux separation can be achieved with low efficiency, while the opposite case gives highly efficient separation with relatively low flux.[18,19] This correlation can also be well explained by the Hagen-Poiseuille equation.[20] On the other hand, coalescence separation is mainly driven by membrane wettability, which can be determined by its chemical composition and structural morphology.[21] In particular, superhydrophilic (the water contact angle on a solid substrate in air ~0°) and underwater superoleophobic (the oil contact angle on a solid substrate in water ~180°) membranes are highly effective for water-permeable and oil-impermeable separations,[22–26] while superoleophilic and underoil superhydrophobic membranes can show the opposite result.[27,28] Furthermore, to maximize separation efficiency, there have been efforts to separate the dispersed phase of emulsions by applying a membrane whose surface is pre-wetted with a continuous phase.[29–31]

Recently, various mesh membranes, such as stainless-steel mesh and copper mesh, have been widely used for oil-water separation due to their highly porous structure and excellent physical/chemical properties.[32–34] By applying surface treatments to the mesh surface, effective separation of emulsions has been reported.[35–38] In particular, various attempts have been made to form secondary thin membranes whose pore sizes are a few micrometers in the mesh holes,[39–42] and the successful separation of fine dispersed droplets through the mesh membranes has also been reported. Nevertheless, the approaches to form the secondary membrane on the mesh hole may require a series of steps that are time-consuming and costly,[43,44] and it might not be adequate for fabricating the membrane with an extremely large area. Accordingly, a more facile approach for the high separation efficiency of emulsions with fine droplets can still be required, and, to meet this demand, we here propose a novel and effective method to separate fine water droplets dispersed in oil via the pre-wetted mesh membrane that still retains significantly larger pores compared to the dispersed droplets.

To effectively achieve pre-wetting of the mesh membranes with water, we here conduct a surface treatment on the mesh surface using TiO_2 nanoparticles. Based on the evaporation and reabsorption of water on the thin film surrounding the mesh wire, the successful formation of a pre-wetted mesh membrane with many empty pores is demonstrated, and the size of pores can even be controlled. Furthermore, based on contact angle measurements, the oleophobic/hydrophilic and underoil hydrophilic characteristics of the mesh surface are identified, strongly indicating that a thin water film can be maintained on the surface of the mesh wire during the separation process. As a result, even though the size of dispersed droplets (~9 μm) is approximately 10 times smaller than the pore size of the mesh (70–130 μm), it is successfully confirmed that a separation efficiency of up to 98% or more can be achieved even through a gravity-driven flow. Lastly, to elucidate the advantages of this newly developed approach, the size and volume fraction of dispersed droplets in the emulsion system are compared with those in previously reported works where mesh membranes have provided extremely high separation efficiency of emulsions.

RESULTS AND DISCUSSION

Surface treatment of the mesh wires using TiO_2 particles and their wetting characteristics

Firstly, after the dipcoating process on the mesh surface with various concentrations of the coating solution, as illustrated in Figure 1A, the surface of the mesh wire is examined by scanning electron microscope (SEM) (Method details). As shown in Figure 1B, the SEM image of the bare mesh clearly indicates a porous structure with an average pore size of 135 μm, and it also exhibits a quite smooth surface of the mesh wire. In the mesh coated with the lowest particle concentration of 0.03 g/mL, the porosity of the mesh seems to be almost identical to that of the bare mesh, but the mesh surface is considerably rough, as indicated in Figure 1C. On the other hand, as the particle concentration of the coating solution increases to 0.06 g/mL and 0.15 g/mL, more particles adhere to the mesh surface. As a result, a thicker particle structure seems to be formed on the mesh surface, and it also grows toward the mesh pores, which significantly reduces the pore size.

To assess the wettability of the mesh membranes, the contact behavior of water droplets on various meshes in air and oil conditions is observed using a customized side-view microscope, as shown in Figure 2A. The contact angles of the droplets are measured within 1~2 s after placing them on the membranes because this short timescale can be relevant to the contact behavior during the actual separation process. Figure 2B shows the change in the contact behavior of water in air with and without the coating. The bare mesh shows ~130° of contact angle, which corresponds to a hydrophobic characteristic, whereas the mesh coated with a particle concentration of 0.03 g/mL exhibits a hydrophilic nature with ~55° of contact angle. Accordingly, it was confirmed that the hydrophobic mesh can be modified into a hydrophilic one through the simple coating process.

According to the Cassie-Baxter equation, $\cos\theta_{eff} = A_m \cos\theta_m + A_c \cos\theta_c$, where θ_m and θ_c are the contact angles for the mesh wire with an area fraction of A_m and for the continuous phase with an area fraction of A_c, respectively. Thus, when the area fractions of the mesh wire and the continuous phase are determined, the water contact angle can be simply estimated. For the C1 case in Figure 2, by substituting the values of A_m, A_c, and θ_c into 0.6, 0.4, and 180° in the aforementioned equation, the contact angle for the mesh wire, θ_m, can be expected to be ~140°. This strongly indicates that, even though the water droplet is placed very close to the surface of the mesh wire, the oil surrounding the wire does not evacuate from the surface, preventing direct contact between the water and the surface. Accordingly, it is confirmed that the bare surface of the mesh wire exhibits a superoleophilic characteristic in an aqueous environment. In contrast, the contact angles for the mesh wires (C2–C4 in Figure 2) whose surfaces are coated with TiO_2-particle solutions are quite different from those of the bare surface. The contact angles of the coated membranes appear to be significantly lower than those of the bare membrane. In particular, as the particle concentration of the coating solution increases from 0.03 g/mL to 0.15 g/mL, the contact angle (θ_{eff}) decreases considerably from ~100° to ~55°. This decrease can be caused by a greater area fraction of the mesh structures with a higher particle concentration, thereby leading to a more hydrophilic

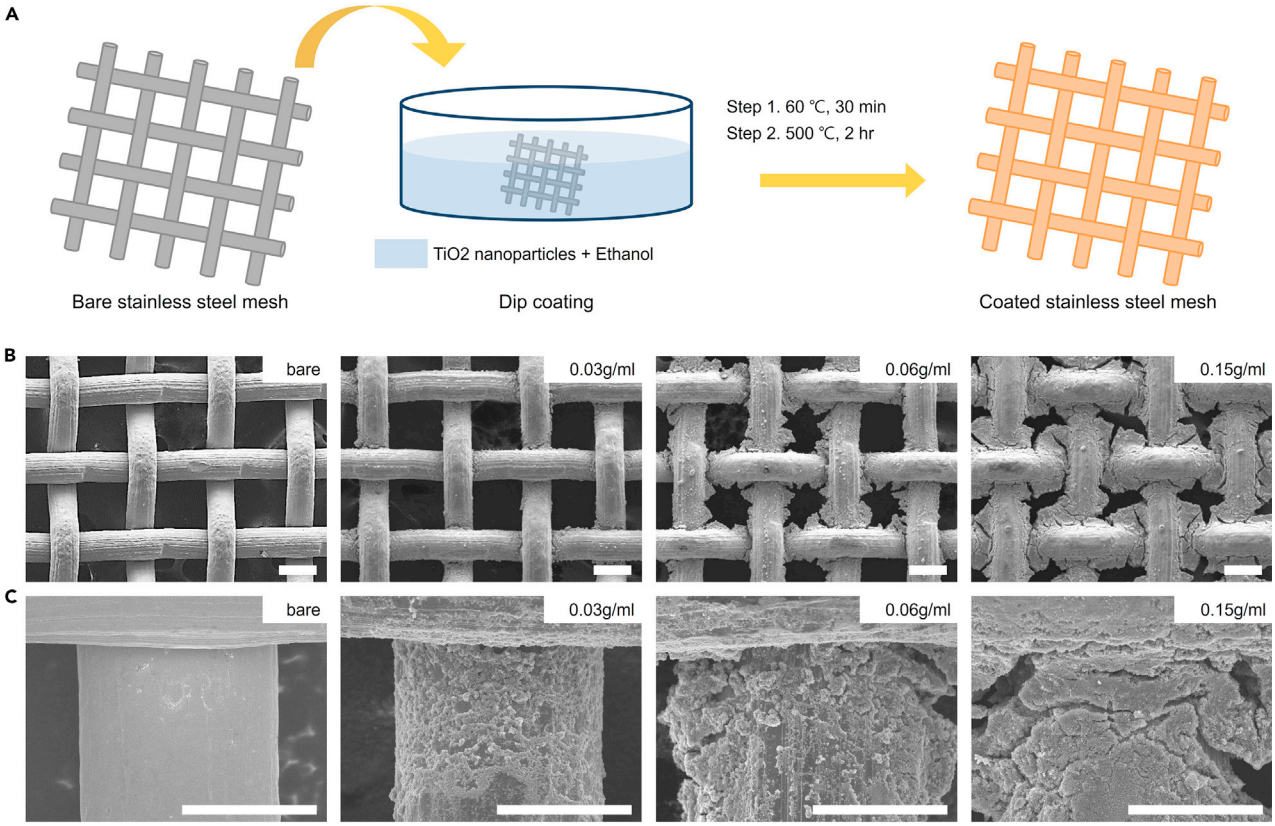

Figure 1. Stainless-steel mesh surface treated with TiO_2 nanoparticles

(A) Schematics depicting the process of dipcoating a bare stainless-steel mesh in a TiO_2-particle solution, solvent evaporation, and sintering to solidly attach the particles to the mesh wire.

(B) SEM images of the bare mesh and the coated meshes with various concentrations of the TiO_2-particle solution.

(C) Magnified SEM images of the mesh surface. Scale bar: (B) 100 μm, (C) 50 μm.

property in the surface of the mesh wire. For example, by applying the Cassie-Baxter equation to the case of C4 in Figure 2, it is expressed as $\cos 55^\circ = 0.89 \cos \theta_m + 0.11 \cos 180^\circ$, thereby resulting in $\theta_{m,C4} \sim 40^\circ$. Consequently, this strongly indicates that the particle-coated mesh surface exhibits a hydrophilic characteristic even when it exists in oil.

Furthermore, the contact behavior of water droplets on the pre-wetted mesh membranes is also investigated. As shown in the D1 of Figure 2, the pre-wetted bare mesh exhibits a contact angle of ~100°, even though the total area of the mesh surface is pre-wetted by water. This occurrence may be attributed to the superoleophilic nature of the bare mesh surface. As the droplets approach the surface, the water surrounding the mesh surface can be expelled, and, instead, oil may preferentially contact the surface directly. This measured effective contact angle aligns well with the estimate from the Cassie-Baxter equation. In contrast, the particle-coated mesh membranes, as previously mentioned in Figure 2B, exhibit hydrophilic characteristics, resulting in the entire membrane appearing to be well-wetted by water. This leads to significantly smaller contact angles, as observed in the D2–D4 images of Figure 2. Here, these small contact angles seem to persist for a few seconds, possibly due to the irregularly wetted membranes, and, after ~10 s, all the small contact angles appear to be zero. Even when a thinner water film is achieved around the mesh wires through an evaporation process, the contact behaviors in E1–E4 of Figure 2 remain almost identical to those in D1–D4 of Figure 2, as shown in Videos S1 and S2. This observation strongly indicates that the thickness of the water film surrounding the mesh wire does not seem to affect the wettability of water droplets on the pre-wetted mesh membranes.

Accordingly, it has been successfully demonstrated that TiO_2 particle-coated mesh membranes exhibit a hydrophilic nature in both air and oil. These intriguing characteristics of the coated mesh surface make it suitable for forming pre-wetted membranes by water and effectively preventing the peeling of thin water films on the mesh surface during the oil penetration process. Therefore, these membranes can be effectively utilized for separating emulsions containing tiny water droplets in oil. While the pre-wetted mesh membranes are expected to offer high separation efficiency, it is important to note that membranes coated with high particle concentrations of 0.06 g/mL and 0.15 g/mL may not be suitable for achieving a relatively high separation flux due to their significantly reduced porosity, as shown in Figure 1B. On the other hand, the mesh membrane coated with a 0.03 g/mL-particle solution exhibits almost the same porosity as that of the bare mesh, while still displaying underoil hydrophilic characteristics, similar to the cases with higher particle concentrations. Therefore, the mesh membrane coated with a particle concentration of 0.03 g/mL is selected for preparing the pre-wetted membrane with water, and subsequent separation processes

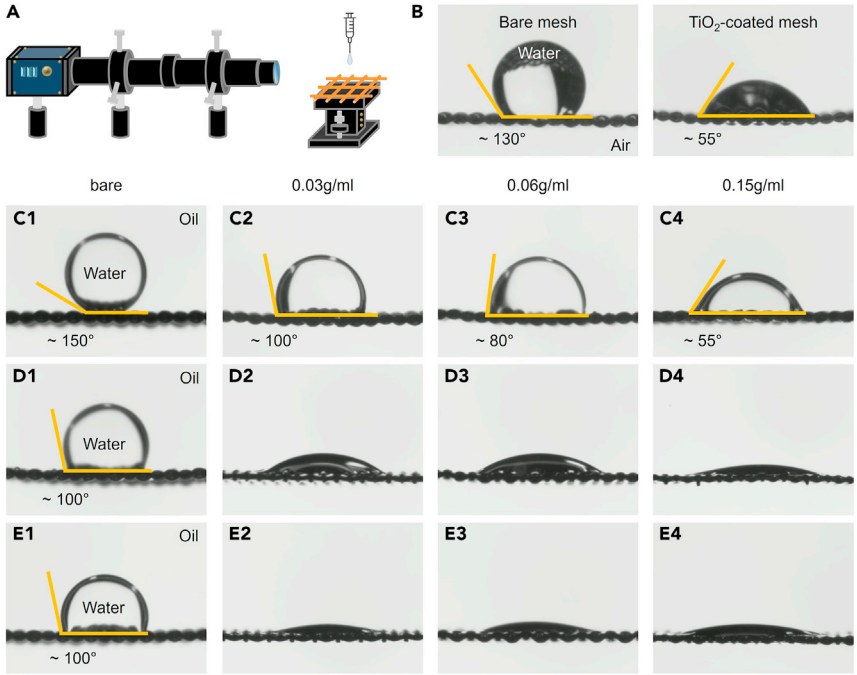

Figure 2. Water contact angle measurement on various mesh membranes

(A) Schematics depicting the method of observing the contact behaviors using a custom-built microscope: In air and underoil contact behaviors of 1 μL-water droplets are observed on the mesh membranes coated with various particle concentrations.

(B) Water droplets on the mesh membranes in air. Here, the TiO_2-coated mesh was coated with a 0.03 g/mL-particle solution. Underoil water droplets (C) on the mesh membranes, (D) on the pre-wetted mesh membranes by water, and (E) on the pre-wetted mesh membranes with a reduced amount of water (50%, compared to D) through evaporation. Labels 1 to 4 indicate the following mesh types in order: the bare, the coated with 0.03 g/mL-, 0.06 g/mL-, and 0.15 g/mL-particle solutions.

are conducted using this pre-wetted membrane. Additionally, it was confirmed that the coated mesh membrane was sufficiently stable under various acid/base conditions (Figure S1).

Morphological changes of the water film via evaporation and reabsorption of water

To achieve high separation efficiency with a relatively high separation flux in the separation of emulsions containing fine water droplets in oil, it is essential to form empty holes in the pre-wetted mesh membrane while still maintaining a thin water film around the mesh wire. The formation of these holes is accomplished through the evaporation of the water residing on the membrane in air (further details are indicated in the Method details). The successful formation of holes is examined by closely observing the morphological changes of the water film on the membrane using confocal laser scanning microscope (CLSM). Specifically, the lateral changes in the morphology of the thin water film on the mesh coated with a 0.03 g/mL particle solution are thoroughly investigated during the evaporation process and compared with the result from the bare mesh membrane, as shown in Figure 3.

As the evaporation process progresses, it becomes evident that the water film residing in the mesh pores gradually becomes thinner, eventually leading to pore openings within 10–15 min after exposure to air (at a temperature of approximately 22–25°C and humidity of approximately 25%–35%), regardless of the type of the mesh membrane. However, the difference between the two mesh membranes becomes apparent when the thin water film creates the pores, as shown in the images in the 4th row of Figures 3A and 3B. In the case of the bare mesh, the thin water film on the mesh wire appears to be completely removed during the evaporation process, whereas the TiO_2-coated mesh maintains the water film on its surface during pore formation. This difference may be attributed to the increased affinity for water resulting from the TiO_2 particle coating on the mesh surface. Furthermore, it is successfully demonstrated that when a considerable amount of water (~0.4 μg/cm^2) is reabsorbed into the water film containing the empty holes, the thickness of the entire water film significantly increases without blocking the holes, as shown in Figure 3C. Consequently, this strongly indicates that the effective pore size of the pre-wetted mesh membrane can be simply controlled by adjusting the amount of water reabsorbed into the water film, potentially having a significant impact on separation efficiency.

Furthermore, the formation of empty holes in the pre-wetted membrane can be more precisely confirmed by estimating the intrusion pressure, which corresponds to the pressure allowing the oil phase to pass through the mesh, as indicated in Figure 4A. It is expected that the intrusion pressure decreases as the thickness of the water film decreases, and, when the empty holes are formed, the intrusion pressure

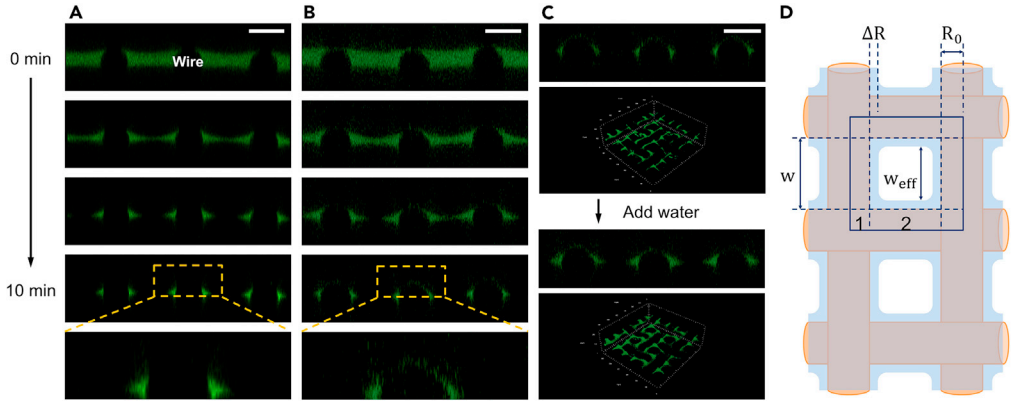

Figure 3. Visualization of morphological changes of the water film surrounding the mesh wires, according to water evaporation, using a CLSM with the addition of 0.01 mg/mL of FITC dye to water

(A) The lateral changes of the water film on the bare mesh.

(B) The lateral change of the water film on the mesh coated with the 0.03 g/mL-particle solution.

(C) Lateral view and slightly tilted top-view images of the pre-wetted mesh structure with empty holes formed by the evaporation of water. (Scale bar: 100 μm).

(D) Illustration of the pre-wetted mesh for the calculation of the effective pore size ($\mathbf{w}_{eff}$). Here, $\mathbf{R}_0$ represents the radius of the mesh wire, $\mathbf{\Delta R}$ is the thickness of the water film, and **w** is the original pore size. 1 and 2 represent divided parts of the mesh wire where part 1 is not related to the effective pore size while part 2 can determine the effective pore size.

immediately reaches a value of zero. Therefore, by measuring the height (h) of the accumulated oil on the pre-wetted mesh membrane just before oil penetration occurs and applying it to the equation $P_{int} = \rho gh$, where ρ and g are the density of hexadecane and the gravitational acceleration constant, respectively, the intrusion pressure (P_{int}) can be simply calculated. The height measurement of the oil accumulated on the pre-wetted mesh is conducted using the customized separation apparatus, as shown in Figure 4B. This apparatus is later utilized for the separation of emulsions containing tiny water droplets.

As a result, based on the controlled water evaporation (see Method details), it is successfully demonstrated that the mass of the water film surrounding the mesh wire gradually decreases with time, indicating a gradual reduction in the thickness of the water film. After 30 min, almost all the water seems to have evaporated completely, as shown in Figure 4C (left). In contrast, considerable intrusion pressures are recorded before evaporation for 15 min (e.g., after 0, 5, and 10 min, intrusion pressures are recorded as ~ 570 Pa, ~460 Pa, and ~250 Pa, respectively). However, the intrusion pressure immediately reaches a value of zero after 15 min, during which approximately 0.053 kg/m^2 of water still remains on the mesh surface, indicating that the empty holes become clearly visible on the pre-wetted mesh at this time. By precisely controlling the water evaporation for 15 min, it is demonstrated that the distinctive morphology of the pre-wetted mesh, where the entire mesh wire is surrounded by a thin water film, but empty holes are clearly observed, can be successfully achieved. Additionally, by adding a considerable amount of water to this pre-wetted mesh, the thickness of the water film surrounding the mesh wire can be controlled, as mentioned in Figure 3C.

Determining the separation efficiency via the pre-wetted mesh membranes

As a model system for the separation, the water-in-oil (W/O)emulsion with an extremely low volume fraction of the dispersed phase (0.125–0.5 vol %) is utilized here, as shown in Figure 5A. Right after the emulsification, the size of dispersed droplets is measured to be ~9 μm, which remains almost identical until an hour after the emulsification. Therefore, this strongly indicates that even though the droplet coalescence can occur upon contact due to the absence of emulsifier, changes in droplet size need not to be considered given that the entire separation process concludes within ~10 min.

Furthermore, it is highly required to quantify the amount of water remaining after the separation, thereby enabling us to effectively estimate the separation efficiency of the emulsion through the pre-wetted mesh membranes, defined by $\frac{Water_{in} - Water_{out}}{Water_{in}} \times 100(\%)$ (See Method details). Accordingly, hydrophilic dye molecules (methylene blue) are initially dissolved in the water phase, and using ultraviolet-visible (UV-vis) spectroscopy, absorbance is then measured with varying the water content in oil. As indicated in Figure 5B, the correlation between the absorbance and the water content is well described by the fitted line of y = 0.0291x (R^2 ~ 0.99), and, based on this calibration curve, the amount of water remaining after the separation can be effectively estimated by measuring absorbance of light at 664 nm of filtrate. (More details are also described in Method details.).

Here, the separation experiments are performed using several different mesh membranes, such as the bare mesh, the coated mesh, and pre-wetted meshes with different amounts of water surrounding the mesh wire (Figure 6A). The pre-wetted meshes are subjected to evaporation and reabsorption of water, resulting in water films with a remaining mass of 44%, 57%, and 65% compared to that of a fully pre-wetted mesh. Furthermore, it should be noted that, during the experiment, some water loss of the emulsion can occur while emulsifying and

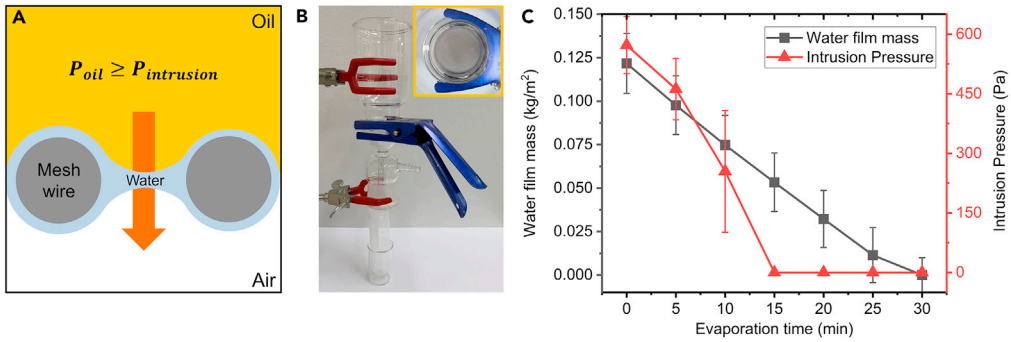

Figure 4. Intrusion pressure of the water-filmed mesh

(A) Schematic illustrating the intrusion pressure for the pre-wetted mesh.

(B) Separation device for measuring the intrusion pressure and conducting the separation experiments, and the top-view image of the device.

(C) Mass change of the water film through evaporation and the change in experimental intrusion pressure according to the water film mass change.

transferring the sample into the separation equipment. Consequently, the amount of the dispersed water phase before the separation ($Water_{in}$) is different from the given mass before the emulsification. Furthermore, there might be some water droplets whose size is comparable to the size of the mesh pore (here, 70–135 μm), with a tiny number fraction in the emulsions sample, and these droplets can be separated by the pore size effect of the bare mesh membrane. Therefore, to precisely quantify the effect of the thin water film surrounding the mesh wire on the separation efficiency, we here set the separation efficiency of the bare mesh membrane as zero.

In comparison to the separation efficiency of the bare mesh membrane, all coated mesh membranes, with and without pre-wetting, provide significantly higher efficiencies, as shown in Figure 6. For example, even in the case of the coated mesh without pre-wetting, it gives 40% greater efficiency, possibly due to the underoil hydrophilic character of the coated mesh surface, resulting in the adsorption of water onto the mesh surface. In contrast, the mesh with 44% water remaining provides slightly higher efficiency (49%) than the just-coated mesh. However, after water reabsorption to the mesh with 44% water remaining, the efficiency increases dramatically to 91% and 98% for the meshes with 57% water and 65% water, respectively. Additionally, the inclusion of a considerable amount of surfactant in the emulsion can lead to decreased separation efficiency, strongly suggesting that the surfactant layer formed on the droplet surface interferes with the absorption of the water droplet into the water film (Figure S2). Here, it should be noted that the total time for all the oil phases to pass through the membrane is measured to estimate the average separation flux. The hydrostatic pressure decreases as the separation progresses, leading to a continuous decrease in instantaneous flux. Instead, measuring the flux within the first 10 s, where the hydrostatic pressure remains similar, can result in a flux of up to 1,140 L/m^2h, even with the mesh membrane with 65% water. Therefore, this approach to measuring separation flux can underestimate the ability of the membrane to achieve high separation flux.

To elucidate the role of the thin water film on the mesh surface in the dramatic increase of separation efficiency, the effective pore size of the meshes is roughly calculated first. As indicated in Method details, the effective pore sizes of the meshes with 44%, 57%, and 65% water are estimated at 86 μm, 75 μm, and 68 μm, respectively, by calculating the thickness of the water film. This estimation is indirectly confirmed by the significantly reduced separation flux values, as shown on the x axis of Figure 6A. Accordingly, it is successfully demonstrated that a smaller effective pore size can considerably increase the separation efficiency with a lower separation flux. However, as the amount of water residing on the mesh surface increases from 44% to 57%, the pore size seems to be gradually decreased, but the separation efficiency changes rapidly. This strongly indicates that the separation efficiency does not seem to be well explained by the effective pore size alone.

Interestingly, despite the presence of the water film, the effective pore sizes of the meshes are still much greater (8–10 times) than those of fine water droplets in emulsions. Unlike solid membranes, the water thin film surrounding the mesh wire can be deformed at a given pressure. The hydrostatic pressure given by the emulsion on the membrane can be simply estimated by ρgh (~76 Pa) where ρ is the density of hexadecane (773 kg/m^3), g is the gravitational acceleration (9.8 kg m/s^2), and h is the height (1 cm when 10 mL is applied) of the emulsion on the membrane. Based on dimensional analysis, the contribution of hydrostatic pressure can be simply estimated by $\rho gh \cdot R_1$ (4.9–15.5 mN/m), where R_1 is the radius of the mesh wire with the thin water film (Figure 6B, Top). This contribution seems to be comparable to the interfacial tension of oil and water (~50 mN/m), which resists the deformation of the water film surrounding the mesh wire. The contribution to deformation can be even greater when the values of h and R_1 increase, thereby resulting in more significant deformation with a thicker water thin film and a larger height of the emulsion on the membrane. Here, it should be noted that contributions from the gravitational deformation of the thin water film ($\sim \rho g \cdot R \cdot \Delta R \sim 0.01$ mN/m) and the deformation by the hydrodynamic pressure ($\sim \frac{1}{2}\rho u^2 < 0.1$ mN/m, here u is simply estimated from the value of the separation flux) are much smaller than those of deformation caused by hydrostatic pressure, so they are neglected.

Accordingly, the deformation of the water thin film may play an important role in determining the separation efficiency. To understand this in more detail, the contact area between the emulsion and the water film (the red line at the bottom of Figure 6B) and the instantaneous effective pore size (W_{eff} in Figure 6B) are roughly calculated during the deformation. Here, it is simply assumed that the upper circle of the cross-sectional area of the mesh wire with water maintains the shape of a semi-circle due to the hydrostatic pressure applied isotropically, but the

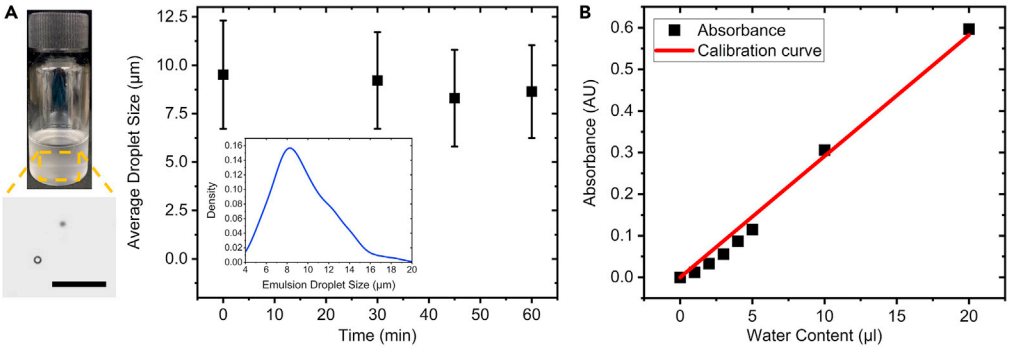

Figure 5. Determination of model emulsion and calibration curve for efficiency calculation

(A) Emulsion containing tiny water droplets in oil and the change in the average size of water droplets with time. (Scale bar: 100 μm. Inset: The size distribution of water droplets, with an average diameter of ~9 μm, immediately after emulsification.).

(B) The calibration curve of absorbance in UV-vis spectroscopy with varying amounts of water in oil. The solid line represents the fitted line of $\mathbf{y = 0.0291x}$, where y and x are the absorbance and the content of water, respectively.

thickness of the water film (R_1) only varies. Therefore, the cross-sectional area of the water film surrounding the upper semi-circle of the mesh wire is expressed as $\frac{\pi(R_1^2 - R_0^2)}{2}$. At the same time, the nearly incompressible hexadecane should move down the lower semi-circle of the cross-sectional area of the mesh wire during the deformation, and, to minimize the total surface area, which results in the minimum total surface energy, another cylindrical water film with R_2 possibly appears below the lower semi-circle, as shown in Figure 6B (bottom). Thus, it is expected that as the magnitude of the hydrostatic pressure increases, R_1 gradually decreases while R_2 increases. Here, the cross-sectional area of the water film surrounding the lower semi-circle of the mesh wire is expressed as $\frac{360^\circ - 2\theta}{360^\circ}(\pi R_2^2) + R_1 R_2 \cos\theta - \frac{\pi R_0^2}{2}$.

Based on this simple cylindrical model, where the cross-sectional area of the water film, $\frac{\pi R_1^2}{2} + \frac{360^\circ - 2\theta}{360^\circ}(\pi R_2^2) + R_1 R_2 \cos\theta - \pi R_0^2$, is required to be constant during the deformation, the effective pore size (Figure 6B) is first estimated at each moment while changing the thickness of the water film on the upper semi-circle of the cross-sectional area of the mesh wire from the initial value to zero. As shown in Figure 7A, the pore size of the mesh wire with 44% water increases initially but gradually decreases after reaching a maximum value, and the mesh wire with 65% water also shows similar behavior of the pore size. Interestingly, despite deformation occurring, the pore size is smallest in the initial stage before applying the pressure, so the deformation does not seem to decrease the pore size. On the other hand, the contact area between water and emulsions, defined in Figure 6B (bottom), indicates quite different behaviors, depending on the initial thickness of the water film. For example, in the case of the mesh wire with 44% water, the contact area increases gradually, and, at zero thickness on the upper semi-circle, it indicates a maximum value (~12% greater than the initial area). However, for the mesh wire with 65% water, it initially increases and then slightly decreases after reaching a maximum value.

When the contact area between the water film and the emulsion greatly increases, the possibility of fine water droplets colliding with the water film can also increase, possibly resulting in better efficiency. Therefore, this suggests that the different behaviors of the contact area may exhibit different trends in the change of separation efficiency with varying hydrostatic pressure. To confirm this, the separation efficiencies in the mesh wires with 44% water and with 65% water are measured while varying the initial height of emulsion on the membrane. Here, 20 mL- and 40 mL-emulsion samples, where the amount of water is kept constant, are prepared to increase the height, which also gives much lower dispersed phase fractions of 0.25 and 0.125 vol %. As shown in Figure 7C, the separation efficiency of the emulsion through the mesh wire with 44% water increases considerably with increasing the emulsion volume, and this trend appears to be similar to the change in contact area (Figure 7B, right). Even when the volume fraction of the dispersed phase is fixed at 0.5 vol %, a similar trend in the separation efficiency still appears (Figure S3A). Additionally, the mesh wire with 65% water provides slightly lower efficiency with increasing volume (Figure 7D), which is also similar to the behavior in Figure 7B (left). This may be due to the deformed interface enough to maximize the efficiency at the hydrostatic pressure given by the 10 mL emulsion. The efficiency tends to decrease more significantly when the 40 mL emulsion with a fixed volume fraction of 0.5 vol % is applied because the amount of dispersed phase in the 40mL emulsion seems to be greater than the maximum absorption capacity of the water film (Figure S3B). Here, it should be noted that despite the change in separation flux from ~50 to ~2,300 L/m^{2}h, these values indicate very low Reynolds numbers (<5), so the separation flux does not seem to have a significant effect on the separation efficiency under these experimental conditions.

So far, various studies have reported the effective separation of emulsions using surface-modified mesh membranes. In most cases, the size of droplets is similar or even larger than the size of the mesh pore, as shown in Figure 8, allowing the separation through a size-sieving mechanism. For example, Zhang et al.[35] and He et al.[36] reported the successful separation of emulsions containing micro-scale droplets using stainless-steel mesh spray-coated with copper particles/aluminum phosphate and copper mesh coated by *in situ*-grown CuC_2O_4 nanosheets, respectively. These approaches provide extremely high efficiency (>99%) for separating the dispersed droplets. However, their utility can be limited when dealing with quite small droplet sizes. Furthermore, when the droplets are clogged in the membrane pores during the separation, the droplets may remain on the membrane even after the separation, thereby continuously degrading the functionality of the

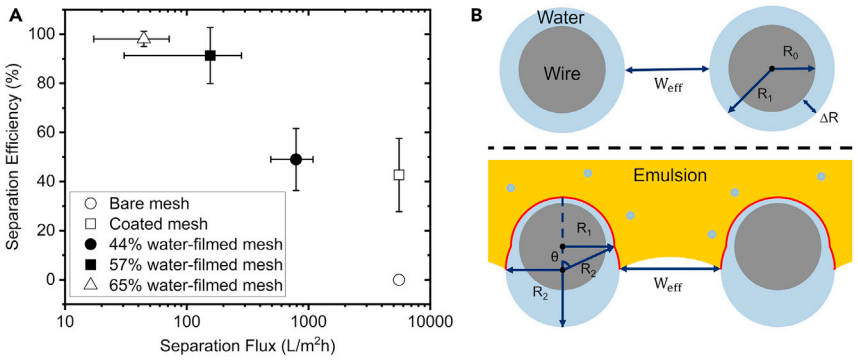

Figure 6. Separation efficiency and flux and the shape change of the water thin film

(A) Variation of the separation efficiency and flux of the emulsion system that contains 0.5 vol % of dispersed water droplets through wetted mesh membranes with varying an amount of water surrounding the mesh wire.

(B) The shape change of the thin water film in the absence (top) and the presence (bottom) of the hydrostatic pressure. Here, R_0 and R_1 are the radius of the mesh wire and the wire with water film whose thickness is ΔR, respectively. R_2 is the radius of the cylindrical structure formed with the deformed water film under the lower semi-circle of the mesh wire. The red solid line represents the contact area between the emulsion and water film.

membrane. As a substitution, Nazarpour Kalaei et al.[37] reported the extremely high separation efficiency (~100%) for emulsions whose droplet size is ~3.5 times smaller than the mesh pore, using stainless-steel grid coated with Mxene nanoparticles. Zuo et al.[38] also achieved effective separation (>95%) of emulsions with droplet size ~5 times smaller than the pore size via Janus stainless-steel mesh coated with polyethyleneimine/aminated carbon nanotubes on both sides. Nevertheless, when comparing the size ratio and the volume fraction to those from other works (Figure 8), it is demonstrated that a significantly larger ratio of the pore size to the droplet size can be achieved while the volume fraction of the dispersed phase is much smaller (down to 0.125). This strongly indicates that this approach can provide greater versatility when applied to the separation of dispersed droplets with varying sizes and volume fractions.

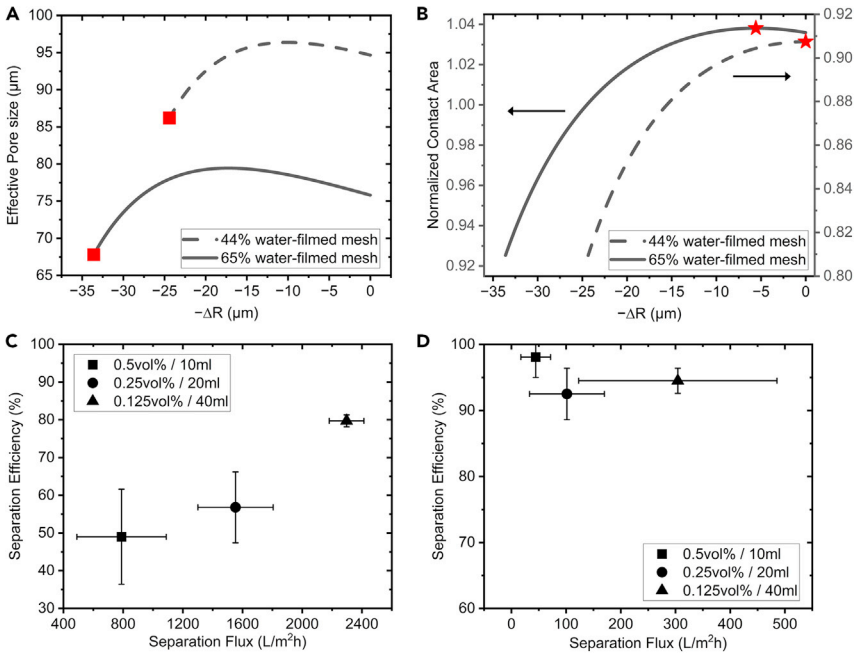

Figure 7. Crucial factors determining the separation efficiency

(A) The changes in the effective pore size (w_{eff}) with varying the water film thickness (**ΔR**) on the upper semi-circle, as described in Figure 6B (bottom), for the meshes with 44% and 65% water, respectively. The red filled squares represent the minimum values of w_{eff} for each case.

(B) The changes in the contact area between the water and the emulsion normalized by the surface area of the bare mesh wire as **ΔR** changes for the meshes with 44% water and 65% water, respectively. The red filled stars indicate the values of the maximum contact area.

(C and D) The results of separating emulsions with higher volumes, 20 mL and 40 mL, by diluting the emulsion from 0.5 vol % to 0.25 vol % and 0.125 vol % (C) through the mesh with 44% water, (D) through the mesh with 65% water.

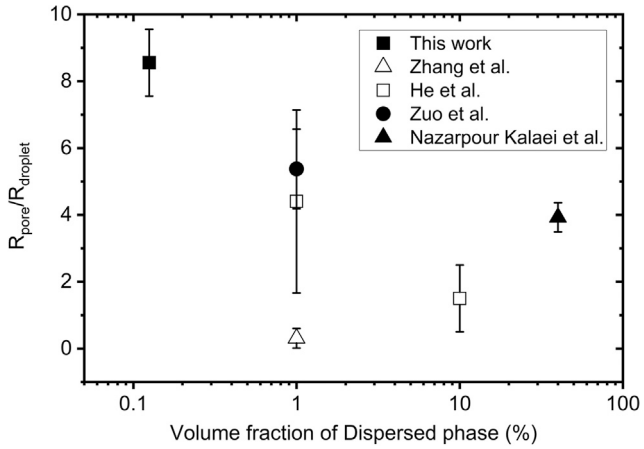

Figure 8. Comparison of separation ability with previous studies

Comparison of the ratio of the pore size to the droplet size (y axis) and the minimum volume fraction of the dispersed phase in the emulsion separation (x axis) with those from Zhang et al. (pore size/droplet size: 0.6 μm/1–40 μm),[35] He et al. (25 μm/10–50 μm, 5 μm/0.7–3 μm),[36] Nazarpour Kalaei et al. (31.4 μm/7.2–9 μm),[37] and Zuo et al. (6.8 μm/1.-1.6 μm).[38] The error bar represents the minimum to maximum value of the y value, and the point represents its median value.

Conclusion

In conclusion, we have demonstrated that effective separation of fine water droplets dispersed in oil can be achieved using the pre-wetted mesh membrane, whose effective pore size is ~10 times greater than the size of droplets, with extremely low volume fractions of the dispersed phase. To obtain the pre-wetted mesh by water, we utilized a stainless-steel mesh with a pore size of 135 μm and coated the mesh surface with TiO_2 nanoparticles to impart hydrophilic and underoil hydrophilic surface characteristics to the mesh wire. Furthermore, based on the water-absorption, evaporation, and water-reabsorption steps, we successfully confirmed that the water thin film surrounding the mesh wire is retained well, and even effective pore size can be controlled.

When applying this membrane to the gravity-driven flow of the emulsion sample, we could achieve an extremely high separation efficiency (>98%). Here, we argued that this high efficiency can possibly be achieved by increasing the interfacial area between the water film and the emulsion during the separation process, as supported by the simple calculations and the experiments. Furthermore, we have successfully demonstrated that our work exhibits unique advantages compared to other separation works utilizing the mesh membranes. These advantages include a greater ratio of the pore size to the droplet size and a lower volume fraction of the dispersed phase in emulsion separation. Therefore, we believe that this new and facile approach can be advantageous for the effective separation of a wide range of emulsion systems, where the size of droplets and the volume fraction of the dispersed droplets are highly variable. Furthermore, it is also expected that this simple approach can be applied effectively in industrial fields where continuous separation processes and extremely large membrane areas are highly required, although more detailed studies and development are still necessary.

Limitations of the study

This method of removing fine water droplets in emulsions achieves high separation efficiencies of over 98% but has mainly focused on emulsion-free emulsions. Further research is needed to separate dispersed water droplets from emulsions containing surfactants and colloidal particles to expand its utilization.

STAR★METHODS

Detailed methods are provided in the online version of this paper and include the following:

- KEY RESOURCES TABLE
- RESOURCE AVAILABILITY
  - Lead contact
  - Materials availability
  - Data and code availability
- METHOD DETAILS
  - Materials
  - Modification of a stainless-steel mesh
  - Characterization of TiO_2-coated meshes
  - Pre-wetting of TiO_2-coated meshes

- Observation of the water thin film
- Determination of the effective pore size
- Measurement of the intrusion pressure
- Preparation of emulsions
- Separation of emulsions
- Determining the separation efficiency

- QUANTIFICATION AND STATISTICAL ANALYSIS

SUPPLEMENTAL INFORMATION

Supplemental information can be found online at https://doi.org/10.1016/j.isci.2024.109556.

ACKNOWLEDGMENTS

This work was supported by the Basic Science Research Program through the National Research Foundation of Korea (NRF-2023R1A2C1006915) and the Material·Component·Technology Development Program (20015430) funded by the Korea Evaluation Institute of Industrial Technology (KEIT, KOREA).

AUTHOR CONTRIBUTIONS

K.K., S.Q.C., and D.K. conceived the idea and designed the research. K.K. and S.Q.C. supervised this study. JiEun Park, E.P., and D.K. performed experiments. JiEun Park, E.P., S.K., D.L., and Jaesung Park analyzed the data. K.K., S.Q.C., D.K., and JiEun Park wrote the manuscripts. All authors commented on the manuscript.

DECLARATION OF INTERESTS

The authors declare no competing interests.

Received: November 14, 2023
Revised: February 8, 2024
Accepted: March 22, 2024
Published: March 23, 2024

REFERENCES

1. Porwal, H.J., Mane, A.V., and Velhal, S.G. (2015). Biodegradation of dairy effluent by using microbial isolates obtained from activated sludge. Water Resour. Ind. *9*, 1–15. https://doi.org/10.1016/J.WRI.2014.11.002.
2. Li, M., and Garrett, C. (1998). The relationship between oil droplet size and upper ocean turbulence. Mar. Pollut. Bull. *36*, 961–970. https://doi.org/10.1016/S0025-326X(98)00096-4.
3. Sørhus, E., Edvardsen, R.B., Karlsen, Ø., Nordtug, T., Van Der Meeren, T., Thorsen, A., Harman, C., Jentoft, S., and Meier, S. (2015). Unexpected Interaction with Dispersed Crude Oil Droplets Drives Severe Toxicity in Atlantic Haddock Embryos. PLoS One *10*, e0124376. https://doi.org/10.1371/JOURNAL.PONE.0124376.
4. Sloan, E.D. (2010). In Natural Gas Hydrates in Flow Assurance (Gulf Professional Publishing), p. 224.
5. Fink, J.K. (2012). Petroleum engineer's guide to oil field chemicals and fluids, *785*.
6. Lesaint, C., Glomm, W.R., Lundgaard, L.E., and Sjöblom, J. (2009). Dehydration efficiency of AC electrical fields on water-in-model-oil emulsions. Colloids Surf. A Physicochem. Eng. Asp. *352*, 63–69. https://doi.org/10.1016/J.COLSURFA.2009.09.051.
7. Kokal, S. (2005). Crude-Oil Emulsions: A State-Of-The-Art Review. SPE Prod. Facil. *20*, 5–13. https://doi.org/10.2118/77497-PA.
8. Anuar Sharuddin, S.D., Abnisa, F., Wan Daud, W.M.A., and Aroua, M.K. (2017). Energy recovery from pyrolysis of plastic waste: Study on non-recycled plastics (NRP) data as the real measure of plastic waste. Energy Convers. Manag. *148*, 925–934. https://doi.org/10.1016/J.ENCONMAN.2017.06.046.
9. Falconer, A., and Metallurgist, S. (2003). Gravity separation: old technique/new methods. Phys. Separ. Sci. Eng. *12*, 31–48. https://doi.org/10.1080/1478647031000104293.
10. Binner, E.R., Robinson, J.P., Silvester, S.A., Kingman, S.W., and Lester, E.H. (2014). Investigation into the mechanisms by which microwave heating enhances separation of water-in-oil emulsions. Fuel *116*, 516–521. https://doi.org/10.1016/J.FUEL.2013.08.042.
11. Comba, M., and Kaiser, K. (1990). Suspended particulate concentrations in the St. Lawrence river (1985–1987) determined by centrifugation and filtration. Sci. Total Environ. *97–98*, 191–206. https://doi.org/10.1016/0048-9697(90)90240-U.
12. Hamamah, Z.A., and Grützner, T. (2022). Liquid-Liquid Centrifugal Extractors: Types and Recent Applications – a Review. ChemBioEng Rev. *9*, 286–318. https://doi.org/10.1002/CBEN.202100035.
13. Mousavichoubeh, M., Shariaty-Niassar, M., and Ghadiri, M. (2011). The effect of interfacial tension on secondary drop formation in electro-coalescence of water droplets in oil. Chem. Eng. Sci. *66*, 5330–5337. https://doi.org/10.1016/J.CES.2011.07.019.
14. Zolfaghari, R., Fakhru'l-Razi, A., Abdullah, L.C., Elnashaie, S.S., and Pendashteh, A. (2016). Demulsification techniques of water-in-oil and oil-in-water emulsions in petroleum industry. Sep. Purif. Technol. *170*, 377–407. https://doi.org/10.1016/J.SEPPUR.2016.06.026.
15. Padaki, M., Surya Murali, R., Abdullah, M.S., Misdan, N., Moslehyani, A., Kassim, M.A., Hilal, N., and Ismail, A.F. (2015). Membrane technology enhancement in oil–water separation. A review. Desalination *357*, 197–207. https://doi.org/10.1016/J.DESAL.2014.11.023.
16. Li, J.R., Sculley, J., and Zhou, H.C. (2012). Metal-organic frameworks for separations. Chem. Rev. *112*, 869–932. https://doi.org/10.1021/CR200190S.
17. Yu, J., Cao, C., Pan, Y., Yu, J., Cao, C., and Pan, Y. (2021). Advances of Adsorption and Filtration Techniques in Separating Highly Viscous Crude Oil/Water Mixtures. Adv. Mater. Interfac. *8*, 2100061. https://doi.org/10.1002/ADMI.202100061.
18. Zhang, G., Jia, X., Xing, J., Shen, S., Zhou, X., Yang, J., Guo, Y., and Bai, R. (2019). A facile and fast approach to coat various substrates with poly(styrene- co-maleic anhydride) and polyethyleneimine for oil/water separation. Ind. Eng. Chem. Res. *58*, 19475–19485. https://doi.org/10.1021/ACS.IECR.9B03465.
19. Wei, W., Sun, M., Zhang, L., Zhao, S., Wu, J., and Wang, J. (2017). Underwater oleophobic PTFE membrane for efficient and reusable

emulsion separation and the influence of surface wettability and pore size. Sep. Purif. Technol. *189*, 32–39. https://doi.org/10.1016/J.SEPPUR.2017.07.074.

20. Baker, R.W., and Richard, W. (2004). Membrane technology and applications, *538*.
21. Erbil, H.Y., Demirel, A.L., Avci, Y., and Mert, O. (2003). Transformation of a simple plastic into a superhydrophobic surface. Science *299*, 1377–1380. https://doi.org/10.1126/SCIENCE.1078365.
22. Sun, Y., Zong, Y., Yang, N., Zhang, N., Jiang, B., Zhang, L., and Xiao, X. (2020). Surface hydrophilic modification of PVDF membranes based on tannin and zwitterionic substance towards effective oil-in-water emulsion separation. Sep. Purif. Technol. *234*, 116015. https://doi.org/10.1016/J.SEPPUR.2019.116015.
23. Yin, X., He, Y., Wang, Y., Yu, H., Chen, J., and Gao, Y. (2020). Bio-inspired antifouling Cellulose nanofiber multifunctional filtration membrane for highly efficient emulsion separation and application in water purification. Kor. J. Chem. Eng. *37*, 1751–1760. https://doi.org/10.1007/S11814-020-0568-4.
24. Kota, A.K., Kwon, G., Choi, W., Mabry, J.M., and Tuteja, A. (2012). Hygro-responsive membranes for effective oil–water separation. Nat. Commun. *3*, 1025–1028. https://doi.org/10.1038/ncomms2027.
25. Xiang, B., Gong, J., Sun, Y., Yan, W., Jin, R., and Li, J. (2024). High permeability PEG/MXene@MOF membrane with stable interlayer spacing and efficient fouling resistance for continuous oily wastewater purification. J. Membr. Sci. *691*, 122247. https://doi.org/10.1016/J.MEMSCI.2023.122247.
26. Xiang, B., Gong, J., Sun, Y., and Li, J. (2024). Robust PVA/GO@MOF membrane with fast photothermal self-cleaning property for oily wastewater purification. J. Hazard Mater. *462*, 132803. https://doi.org/10.1016/J.JHAZMAT.2023.132803.
27. Xu, H., Liu, H., Huang, Y., and Xiao, C. (2021). Three-dimensional structure design of tubular polyvinyl chloride hybrid nanofiber membranes for water-in-oil emulsion separation. J. Membr. Sci. *620*, 118905. https://doi.org/10.1016/J.MEMSCI.2020.118905.
28. Zhou, F., Wang, Y., Dai, L., Xu, F., Qu, K., and Xu, Z. (2022). Anchoring metal organic frameworks on nanofibers via etching-assisted strategy: Toward water-in-oil emulsion separation membranes. Sep. Purif. Technol. *281*, 119812. https://doi.org/10.1016/J.SEPPUR.2021.119812.
29. Wang, W., Mou, L., Yang, D., Wang, Y., and Yang, F. (2022). Construction of superhydrophilic and underwater superoleophobic corn stalk/konjac glucomannan aerogel for high-efficiency oil/water emulsion separation. Kor. J. Chem. Eng. *39*, 2664–2674. https://doi.org/10.1007/S11814-022-1133-0.
30. Li, L., Xu, Z., Sun, W., Chen, J., Dai, C., Yan, B., and Zeng, H. (2020). Bio-inspired membrane with adaptable wettability for smart oil/water separation. J. Membr. Sci. *598*, 117661. https://doi.org/10.1016/J.MEMSCI.2019.117661.
31. Zhang, N., Yang, N., Zhang, L., Jiang, B., Sun, Y., Ma, J., Cheng, K., and Peng, F. (2020). Facile hydrophilic modification of PVDF membrane with Ag/EGCG decorated micro/nanostructural surface for efficient oil-in-water emulsion separation. Chem. Eng. J. *402*, 126200. https://doi.org/10.1016/J.CEJ.2020.126200.
32. Song, J., Huang, S., Lu, Y., Bu, X., Mates, J.E., Ghosh, A., Ganguly, R., Carmalt, C.J., Parkin, I.P., Xu, W., and Megaridis, C.M. (2014). Self-driven one-step oil removal from oil spill on water via selective-wettability steel mesh. ACS Appl. Mater. Interfaces *6*, 19858–19865. https://doi.org/10.1021/AM505254J.
33. Zhang, L., Zhong, Y., Cha, D., and Wang, P. (2013). A self-cleaning underwater superoleophobic mesh for oil-water separation. Sci. Rep. *2326–2335*. https://doi.org/10.1038/srep02326.
34. Crick, C.R., Gibbins, J.A., and Parkin, I.P. (2013). Superhydrophobic polymer -coated copper-mesh; membranes for highly efficient oil–water separation. J. Mater. Chem. A Mater. *1*, 5943–5948. https://doi.org/10.1039/C3TA10636E.
35. Zhang, J., Zhu, L., Zhao, S., Wang, D., and Guo, Z. (2021). A robust and repairable copper-based superhydrophobic microfiltration membrane for high-efficiency water-in-oil emulsion separation. Sep. Purif. Technol. *256*, 117751. https://doi.org/10.1016/j.seppur.2020.117751.
36. He, H., Zhang, T.C., Li, Z., Liang, Y., and Yuan, S. (2021). Superhydrophilic fish-scale-like CuC2O4 nanosheets wrapped copper mesh with underwater super oil-repellent properties for effective separation of oil-in-water emulsions. Colloids Surf. A Physicochem. Eng. Asp. *627*, 127133. https://doi.org/10.1016/J.COLSURFA.2021.127133.
37. Nazarpour Kalaei, M.R., Heydarinasab, A., Rashidi, A., and Alaei, M. (2023). Facile fabrication of Mxene coated metal mesh-based material for oil/water emulsion separation. Ecotoxicol. Environ. Saf. *255*, 114824. https://doi.org/10.1016/J.ECOENV.2023.114824.
38. Zuo, J., Zhou, Y., Chen, Z., Zhao, T., Tan, Q., Zhou, C., Zeng, X., Xu, S., Cheng, J., Wen, X., and Pi, P. (2022). A superwetting stainless steel mesh with Janus surface charges for efficient emulsion separation. J. Hazard Mater. *430*, 128378. https://doi.org/10.1016/J.JHAZMAT.2022.128378.
39. Lin, X., Choi, M., Heo, J., Jeong, H., Park, S., and Hong, J. (2017). Cobweb-Inspired Superhydrophobic Multiscaled Gating Membrane with Embedded Network Structure for Robust Water-in-Oil Emulsion Separation. ACS Sustain. Chem. Eng. *5*, 3448–3455. https://doi.org/10.1021/ACSSUSCHEMENG.7B00124.
40. Song, P., and Lu, Q. (2020). Porous clusters of metal-organic framework coated stainless steel mesh for highly efficient oil/water separation. Sep. Purif. Technol. *238*, 116454. https://doi.org/10.1016/J.SEPPUR.2019.116454.
41. Wang, H., Li, J., Yu, X., Zhao, X., Zeng, X., Xu, F., Tang, X., Sun, Y., and Lin, L. (2021). Facile fabrication of super-hydrophilic cellulose hydrogel-coated mesh using deep eutectic solvent for efficient gravity-driven oil/water separation. Cellulose *28*, 949–960. https://doi.org/10.1007/S10570-020-03578-9.
42. Li, H., Zhu, G., Shen, Y., Han, Z., Zhang, J., and Li, J. (2019). Robust superhydrophobic attapulgite meshes for effective separation of water-in-oil emulsions. J. Colloid Interface Sci. *557*, 84–93. https://doi.org/10.1016/J.JCIS.2019.09.013.
43. Liu, N., Lin, X., Zhang, W., Cao, Y., Chen, Y., Feng, L., and Wei, Y. (2015). A Pure Inorganic ZnO-Co3O4 Overlapped Membrane for Efficient Oil/Water Emulsions Separation. Sci. Rep. *5*, 9688–9696. https://doi.org/10.1038/srep09688.
44. Zuo, J., Liu, Z., Zhou, C., Zhou, Y., Wen, X., Xu, S., Cheng, J., and Pi, P. (2021). A durable superwetting clusters-inlayed mesh with high efficiency and flux for emulsion separation. J. Hazard Mater. *403*, 123620. https://doi.org/10.1016/J.JHAZMAT.2020.123620.
45. Jo, S., and Kim, Y. (2016). Superhydrophilic–underwater superoleophobic TiO2-coated mesh for separation of oil from oily seawater/wastewater. Kor. J. Chem. Eng. *33*, 3203–3206. https://doi.org/10.1007/S11814-016-0184-5.
46. Gondal, M.A., Sadullah, M.S., Dastageer, M.A., McKinley, G.H., Panchanathan, D., and Varanasi, K.K. (2014). Study of factors governing oil-water separation process using TiO 2 films prepared by spray deposition of nanoparticle dispersions. ACS Appl. Mater. Interfaces *6*, 13422–13429. https://doi.org/10.1021/AM501867B.
47. Milne, A.J.B., and Amirfazli, A. (2012). The Cassie equation: How it is meant to be used. Adv. Colloid Interface Sci. *170*, 48–55. https://doi.org/10.1016/J.CIS.2011.12.001.
48. Emadzadeh, D., Lau, W.J., Matsuura, T., Rahbari-Sisakht, M., and Ismail, A.F. (2014). A novel thin film composite forward osmosis membrane prepared from PSf–TiO2 nanocomposite substrate for water desalination. Chem. Eng. J. *237*, 70–80. https://doi.org/10.1016/J.CEJ.2013.09.081.
49. Regan, J.O., and Mulvihill, D.M. (2009). Water soluble inner aqueous phase markers as indicators of the encapsulation properties of water-in-oil-in-water emulsions stabilized with sodium caseinate. Food Hydrocolloids *23*, 2339–2345. https://doi.org/10.1016/J.FOODHYD.2009.06.009.

STAR★METHODS

KEY RESOURCES TABLE

REAGENT or RESOURCE	SOURCE	IDENTIFIER
Chemicals, peptides, and recombinant proteins		
Methylene blue hydrate	Sigma-Aldrich	Cat#66720
Titanium(IV) oxide	Sigma-Aldrich	Cat#718467
Span® 80	Sigma-Aldrich	Cat#S6760
Stainless steel mesh	Anping County Bolin Metal Wire Mesh Co., Ltd	Cat#110x110
Fluorescein isothiocyanate–dextran	Sigma-Aldrich	Cat#FD40S
n-Hexadecane, 95%	Thermo scientific	Cat#043283.LV
Software and algorithms		
Origin	OriginLab Corporation.	https://www.originlab.com/
ImageJ	NIH	https://imagej.net/ij/
Other		
LSM 800 BIO CLSM	Carl Zeiss	https://www.micro-shop.zeiss.com/en/kr/shop/search/lsm%20800
SU8010 HR-SEM	Hitachi High Technologies Corporation	https://www.hitachi-hightech.com/global/en/products/microscopes/sem-tem-stem/fe-sem/
BX53M Optical microscope	Olympus	https://www.olympus-lifescience.com/ko/microscopes/upright/bx53f2/
UVmini-1240 UV-Vis spectrophotometer	Shimadzu	https://www.shimadzu.co.kr/products/molecular-spectroscopy/uv-vis/uv-vis-nir-spectroscopy/index.html

RESOURCE AVAILABILITY

Lead contact

Further information and requests for resources and reagents should be directed to and will be fulfilled by the lead contact, KyuHan Kim (kyuhankim@seoultech.ac.kr).

Materials availability

This study did not generate new unique reagents.

Data and code availability

- Authors declare the data are included in the paper and supplemental information files.
- This study does not report any original code.
- Any additional information required to reanalyze the data reported in this paper is available from the lead contact upon request.

METHOD DETAILS

Materials

The stainless steel mesh was purchased from Anping County Bolin Metal Wire Mesh Co., Ltd (China). Methylene blue hydrate, titanium oxide (TiO_2), span 80, and fluorescein isothiocyanate-dextran (FITC) were purchased from Sigma-Aldrich. Hexadecane (95 %) was purchased from Thermo Scientific. Sodium hydroxide beads, ethyl alcohol (Extra Pure) and acetone (Extra Pure) were purchased from Daejung Chemicals & Metals (South Korea). Hydrochloric acid was purchased from Samchun Chemical (South Korea). All of these were used without further purification. Deionized water (DI water, 18.2 mΩ·cm) was utilized here and obtained from a water purification system (Human Corporation, South Korea).

Modification of a stainless-steel mesh

After cutting the stainless-steel mesh, which has an average pore size is 135 μm, into a size of 5 cm × 5 cm, it was washed using ultrasonic treatments (WUC-D06H, DAIHAN scientific) in DI water and acetone for 30 minutes each. The coating process followed a previously reported method,[45] as shown in Figure 1A. The coating solution was prepared by dispersing TiO_2 nanoparticles in ethanol using a vortex mixer (MaXshake™ VM30, DAIHAN Scientific). The solutions were prepared at three different concentrations: 0.03 g/ml, 0.06 g/ml, and 0.15 g/ml, respectively. The coating proceeded through a dip coating method, wherein the mesh was immersed in the coating solution for 10 seconds, then taken out and gently shaken to remove the excess solution. After the dip coating, the mesh was heat-treated for 30 minutes in a dry oven at 60°C and 2 hours in a sintering furnace at 500°C, respectively. This heat treatment dried the solution, improved crystallinity, and made the surface mechanically robust.[46]

Characterization of TiO_2-coated meshes

The mesh surface was observed using a high-resolution scanning electron microscope (HR-SEM, SU8010, Hitachi High Technologies Corporation), as shown in Figures 1B and 1C. The wettability of the mesh was confirmed by sessile drop contact angle measurement. The droplet volume was fixed at 1 μl, and the behavior of the droplet on the mesh membrane was observed using a customized side-view microscope (Figure 2). To evaluate the wettability of the coated mesh surface, the Cassie-Baxter equation, $\cos\theta_{eff} = A_m \cos\theta_m + A_c \cos\theta_c$,[47] was applied. ($A_m$: area fraction of the mesh wire, A_c: area fraction of continuous phase, θ_{eff}: effective water contact angle measured by optical microscope, θ_m: calculated water contact angle on the mesh wire surface, and θ_c: water contact angle with continuous phase) In the equation, area fractions were obtained by analyzing the SEM image of the mesh membrane using a ImageJ program. To evaluate the stability of the mesh membrane when exposed to acids and bases, the coated mesh was immersed in various pH solutions for 24 hours. These aqueous solutions with various pH levels were prepared using 1M-aqueous solutions of hydrochloric acid and sodium hydroxide.

Pre-wetting of TiO_2-coated meshes

Pre-wetting was carried out by immersing the mesh in DI water for 10 seconds and then waiting for all the water droplets to fall off from the mesh after taking it out of the water, repeating the process three times. In order to form the pores in pre-wetted mesh membranes, the water film was then evaporated by placing the pre-wetted mesh in the acrylic container with silica gel inside (24cm*24cm*24cm), in which the temperature and humidity were maintained at 22°C and 20-25 %, respectively.

Observation of the water thin film

The thin water film formed on the surface of bare and coated meshes by the pre-wetting process was observed using a confocal laser scanning microscope (CLSM, LSM 800 BIO, Carl Zeiss), as shown in Figures 3A–3C. Here, the fluorescent reagent FITC dye (excited at a wavelength of 448 nm and emitted at a wavelength of 520 nm, Sigma-Aldrich) was used to visualize the water phase. Each pre-wetted mesh sample, sized at 11 mm × 11 mm, was prepared with an FITC aqueous solution at a concentration of ~ 0.01 mg/ml. Since the bare mesh was hydrophobic, it was sonicated for 1 minute in the aqueous FITC solution to effectively fill the mesh pores with the solution. In contrast, the TiO_2-coated mesh was prepared only by immersion, as the solution penetrated well without any additional treatment. The CLSM images were obtained by irradiating a 488 nm laser (10 mW) with a 10x lens at a temperature of ~ 22°C, and a humidity of 25-35 %. Furthermore, the meniscus of the water film was also captured by scanning the x-y plane in the z direction, and the image-stacking process along the z direction took ~ 1 min.

Determination of the effective pore size

For the pre-wetted mesh membranes, the effective pore size (w_{eff}) was approximately calculated following the procedure below. First, a unit cell was defined, as shown by the solid line in Figure 3D. It was assumed that the mesh wire diameter remains constant with a value of 79 μm across the entire area, and the wire in the unit cell was divided into two different parts: 1) a part that is not related to determining the effective pore size and 2) a part that is closely concerned with determining the effective pore size after the pre-wetting process. For the mesh without the pre-wetting process, the volume of part 1 within the unit cell is calculated as $\sim 4 \times (R_0^2 \times 2R_0)$, and the volume of part 2 can be calculated as $\sim 4 \times \frac{\pi R_0^2 \times w}{2}$. Here, R_0 represents the radius of the mesh wire (~ 39.5 μm), and w is the original pore size (~ 135 μm). The total wire volume of the unit cell is the sum of these two parts, corresponding to $\sim 1.8 \times 10^6\ \mu m^3$.

Considering the pre-wetted mesh membranes whose wire is surrounded by the water thin film with 44% remaining mass relative to its mass immediately after the pre-wetting process, achieved through pre-wetting and evaporation, the volume of the water thin film is estimated to be $1.028 \times 10^{11}\ \mu m^3$. Here, the total area of the mesh membrane is $\pi(2.5cm)^2 \sim 1.9 \times 10^9 \mu m^2$, and the unit cell area is given by $(w+2R_0)^2 \sim 4.6 \times 10^4 \mu m^2$, thereby providing that $\sim 4.2 \times 10^4$ numbers of unit cells exist in the total membrane. Thus, the volume of water assigned to a single unit cell is $\sim 2.4 \times 10^6\ \mu m^3$. As a result, the total volume of a unit cell with the thin water film, whose thickness is ΔR, is $\sim 4.2 \times 10^6\ \mu m^3$, and this can also be given by $4 \times ((R_0+\Delta R)^2 \times 2(R_0 + \Delta R)) + 4 \times \frac{\pi(R_0+\Delta R)^2 \times w}{2}$, thereby resulting in $R_0 + \Delta R \sim 64\ \mu m$, and the effective pore size ($w_{eff} = w - 2\Delta R$) is $\sim 86\ \mu m$. Based on the same procedures, w_{eff} values can be calculated for the other meshes surrounded by water with remaining masses of 57% and 65%, resulting in $\sim 75\ \mu m$ and $\sim 68\ \mu m$, respectively.

Measurement of the intrusion pressure

As shown in Figure 4B, the emulsion separation device is prepared by clamping the top-glass tube and glass funnel onto a stand and inserting the mesh between them. Using the separation device, the change in intrusion pressure was measured for various water film thicknesses. The water film thickness was controlled by changing the evaporation time and was quantified as weight per unit area by measuring the mass at 5-minute intervals (Figure 4C, left). Then, the water-filmed mesh was applied to the separation device, and pure hexadecane was placed on top of it in increments of 10 ml to check the oil height (h) at which oil starts to flow. By applying the height to the equation, $P_{int} = \rho gh$,[46] where ρ and g are the density of hexadecane and the gravitational acceleration constant, respectively, the intrusion pressure (P_{int}) can be simply calculated (Figure 4C, right).

Preparation of emulsions

The emulsion was produced by emulsifying 10 ml of hexadecane with 0.05 ml of the water phase containing methylene blue dye molecules at a concentration of 0.00025 wt% for 210 seconds at 10,000 rpm using a homogenizer (HG-15D, DAIHAN Scientific). Due to the extremely low volume fraction of the dispersed phase (0.125-0.5 vol%), no surfactant was added during the emulsification. Here, the emulsions were stable without significant changes in droplet size for at least 30 minutes, as shown in Figure 5A. Thus, during the separation process, the coalescence of droplets due to the lack of surfactants has not been considered here. The emulsion droplets were observed using an optical microscope (BX53M, Olympus), and their size was analyzed with the ImageJ program.

Emulsions containing surfactants were prepared by adding an oil phase containing surfactants to a preformed emulsion. Specifically, to form the emulsion, 50 μl of a dye aqueous solution was added to 9.9 ml of hexadecane and homogenize at same condition of surfactant-free emulsion production. Then, 0.1 ml of the hexadecane phase containing span 80 at concentrations of × 100-CMC (5 mg/ml) and × 1000-CMC (50 mg/ml) was added to the preformed emulsions, resulting in emulsions of X1-CMC and X10-CMC, respectively. It should be noted that the emulsions were formed through the multi-step process to maintain the droplet size similar to that of surfactant-free emulsions.

Separation of emulsions

To proceed with the separation, the emulsion sample of 10 ml was first flowed onto the membrane. The sample was poured gently to minimize damage to the water film surrounding the mesh wire. The sample that passed through the mesh was collected in a conical tube positioned under a glass funnel. The separation flux, J, was calculated using the following equation, $J = \frac{V}{t \cdot A}$ (L/m^2h).[48] In this equation, V represents the volume of the sample to be separated, t is the time to complete the separation process, and A is the filtration area. Here, when estimating the separation efficiency, each mesh was used for at most 20 separation processes. Indeed, it was indirectly confirmed that the amount of water film on the mesh surface can be maintained before and after the separation under appropriate conditions (Figure S4).

Determining the separation efficiency

To determine the separation efficiency, quantifying the amount of the dispersed phase remaining after separation is essential. To do so, a UV-Vis spectrophotometer (UVmini-1240, Shimadzu) was utilized, especially measuring the absorbance at 664 nm, which is the wavelength at the absorption peak of methylene blue in aqueous solution. To effectively determine the amount of the dispersed water phase in oil, mixtures of 10 ml hexadecane with various water content (1, 2, 3, 4, 5, 10, and 20 μl) were prepared and emulsified with 0.065 wt% span 80 in hexadecane (~10 times greater than CMC) for 3 minutes using a vortex mixer (~ 2000 rpm). Their absorbance was then measured at 664 nm, and the calibration curve, showing the correlation between the content of the aqueous solution in oil and absorbance, was successfully established, as shown in Figure 5B.

Based on the calibration curve, the amount of water remaining after separation could be simply estimated, and the separation efficiency was then calculated by $(Water_{in} - Water_{out})/Water_{in} \times 100$ (%). Here, $Water_{in}$ and $Water_{out}$ represent the amount of the water phase in the emulsion before and after the separation, respectively. It should be noted that the adsorption of methylene blue to oil and the interface was neglected because it is known that methylene blue is only soluble in water,[49] and as a result, we believe that the concentration of methylene blue in the aqueous solution remains constant during the separation process.

QUANTIFICATION AND STATISTICAL ANALYSIS

There is no statistical analysis in this study.